Journal of Photochemistry and Photobiology A: Chemistry 224 (2011) 110–115

Contents lists available at SciVerse ScienceDirect

Journal of Photochemistry and Photobiology A: Chemistry

journal homepage: www.elsevier.com/locate/jphotochem

Blue and green luminescence from layered zinc hydroxide/dodecyl sulfate hybrid nanosheets

Changhao Liang[a,*], Zhenfei Tian[a], Tohru Tsuruoka[b], Weiping Cai[a], Naoto Koshizaki[c]

[a] Key Laboratory of Nanomaterials and Nanotechnology, Institute of Solid State Physics, Hefei Institutes of Physical Science, Chinese Academy of Sciences, Hefei 230031, China
[b] International Center for Materials Nanoarchitectonics (MANA), National Institute for Materials Science, 1-1 Namiki, Tsukuba, Ibaraki 305-0044, Japan
[c] Nanotechnology Research Institute (NRI), National Institute of Advanced Industrial Science and Technology (AIST), Central 5, 1-1-1 Higashi, Tsukuba, Ibaraki 305-8565, Japan

ARTICLE INFO

Article history:
Received 26 April 2011
Received in revised form 16 August 2011
Accepted 9 September 2011
Available online 16 September 2011

Keywords:
Blue photoluminescence
Hybrid nanosheet
β-$Zn(OH)_2$
Laser ablation in liquid
Self-assembly

ABSTRACT

A plasma plume consisting of metal ions and atoms induced by laser ablation of metal Zn can react strongly with the molecules it encounters in liquid solutions. We report the liquid-phase laser ablation-induced synthesis of ZnO nanoparticles and layered zinc hydroxide/dodecyl sulfate (ZnHDS) hybrid nanosheets using a fundamental 1064-nm nanosecond laser. A large amount of ZnHDS nanosheets, together with a small amount of Zn nanospheres and ZnO nanoparticles, could be produced from sodium dodecyl sulfate (SDS) solutions. Thermally induced vaporization of Zn species is favorable for the formation of ZnHDS nanosheets in SDS solutions and ZnO nanoparticles in pure water, while the explosive boiling and ejection of melting Zn droplets is responsible for the formation of sphere-like Zn particles. Photoluminescence measurements of ensemble or individual ablated products reveal that hybrid ZnHDS nanosheets assembled from metastable β-$Zn(OH)_2$ and DS^- ions show strong blue and green luminescence under UV-light excitation.

1. Introduction

Over the past few decades, laser ablation in liquids (LAL) has aroused great interest in the production of various nanoparticles and assembly of complex nanostructures [1,2]. The advantages of a chemically clean synthesis procedure that can be applied to almost any material and liquid solvent are of great benefit to a broad range of nanostructures [3–5], including explorations of their native size and structure-dependent properties, and their utilization in various environmental [6,7] and biomedical applications [8,9]. When using active metals or compounds as targets, strong reactions may occur between the ablated plasma plume and the solution molecules it encounters because the most nascent ablation species of active metal targets are electronically excited and highly reactive. The nanomaterials produced depend on the way materials are liberated from the target, and the reactions between the ejected species and solutions [10–15].

Laser ablated Zn in liquids could be one of the most-studied materials among metals [16–21]. The charging assembly of layered zinc hydroxide/dodecyl sulfate (ZnHDS) nanocomposites in sodium dodecyl sulfate (SDS) solutions and the fabrication of ZnO nanoparticles in deionized water using the third harmonic line (355 nm) of an Nd:YAG laser have been reported [16]. Zn nanoparticles in a pure organic solution of tetrahydrofuran could be formed using a picosecond-pulsed laser [20]. However, no reports about the formation of ZnHDS nanosheets using fundamental (1064 nm) nanosecond pulse laser are currently available, and the optical properties of LAL-induced layered ZnHDS nanosheets have not been investigated. ZnO-based hybrid structures, such as ZnO/poly(ethylene glycol), hybrid materials based on oligothiophene acids and ZnO, ZnO-ILCs nanocrystals, and polyether-grafted ZnO nanoparticle, have been recently reported [22–25]. However, the underlying mechanism of blue emissions remains unclear. The UV and green band emissions of semiconductor ZnO are usually observable, but the blue emission of pure ZnO is not. Basic solutions of LiOH or NaOH are required to prepare ZnO-based hybrid structures. Blue luminescence with enhanced intensity can only be observed at very high LiOH concentrations in ZnO/poly(ethylene glycol) composites [22]. The oxolation reaction, in which a Zn–O–Zn bridge similar to that during ZnO formation is produced, is known to require strong basic conditions. In a weakly basic medium, olation may occur, leading to the formation of the Zn–(OH)–Zn bridge. Therefore, it is reasonable to speculate that the blue emission of ZnO may be related to the surface bonding of OH radicals. Layered ZnO films intercalated with DS^- ions have recently been reported

* Corresponding author. Tel.: +86 551 5591129; fax: +86 551 5591434.
E-mail address: chliang@issp.ac.cn (C. Liang).

1010-6030/$ – see front matter © 2011 Elsevier B.V. All rights reserved.
doi:10.1016/j.jphotochem.2011.09.013

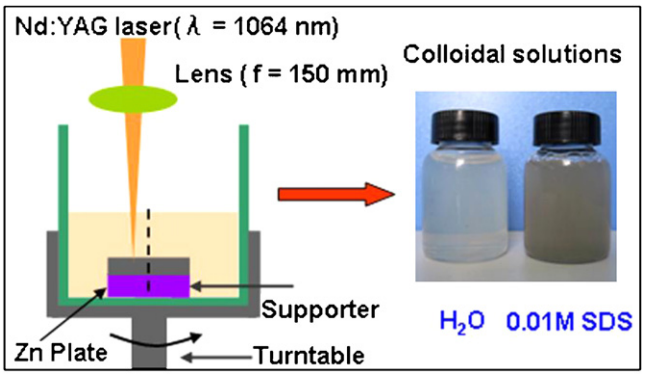

Scheme 1. Experimental design and products of liquid-phase laser ablation of Zn.

to show only the typical photoluminescence (PL) of UV and green-bands without blue emission, as in ZnO nanoparticles [26]. In the current paper, we report that zinc hydroxide (β-$Zn(OH)_2$) intercalated with DS^- ions, which produces layered hybrid nanosheets, can emit strong and stable blue and green light under UV-light excitation.

We demonstrate here the facile formation of a large amount of layered zinc hydroxide/dodecyl sulfate hybrid nanosheets by laser ablation of Zn in water and SDS solutions using a 1064-nm laser. Scanning near-field optical microscopy (SNOM), a powerful tool for investigating the optical properties of single nanostructures [27,28] shows photoemissions from hybrid nanosheets detected not only in ensemble products, but also in individual ones.

2. Experimental

2.1. Liquid-phase laser ablation of Zn

As schematically illustrated in Scheme 1, a Zn (99.99%) plate was fixed to the bottom of a glass vessel filled with 7–10 cm^3 0.01 M sodium dodecyl sulfate (SDS) solution or pure deionized water (>18 MΩ). The target surface was thoroughly cleaned by ultrasonication in ethanol before ablation. Ablation was carried out at normal incidence using a pulsed Nd:YAG laser operating at the fundamental frequency (1064 nm) with a repetition rate of 10 Hz and a pulse duration of 10 ns. The laser was focused on the target with a spot size of about 1 mm in diameter. The laser ablation lasted for 30 min, with a typical 70 mJ/pulse energy near the surface of target. The glass vessel containing the target and solutions was rotated at about 10 rpm during the ablation. After ablation, the SDS solution in the bottle changed into a cloudy, dark gray liquid, whereas the pure water in the other bottle changed into a white liquid, as shown in the imaged beakers of Scheme 1. A large amount of flocculate products was obtained from the SDS solution, whereas small amount of deposits formed in the pure water after settling, as shown in Fig. S1 of the Supplementary Data. The powder samples were then collected by repeated centrifugation, rinsing, and drying at room temperature. Due to the good solubility of SDS molecules in water, excess or unreacted SDS molecules could be removed after repeatedly rinsing.

2.2. Structure and morphology characterization

The collected powder was directly investigated by X-ray diffraction (XRD) using a Philips X'Pert system with CuKα radiation (λ = 1.5419 Å, scanning rate 1.0°/min). The morphology and structure of the products were examined by scanning electron microscopy (SEM) and transmission electron microscopy (TEM) (JEOL, JEM-2010) with an acceleration voltage of 200 kV. Specimens

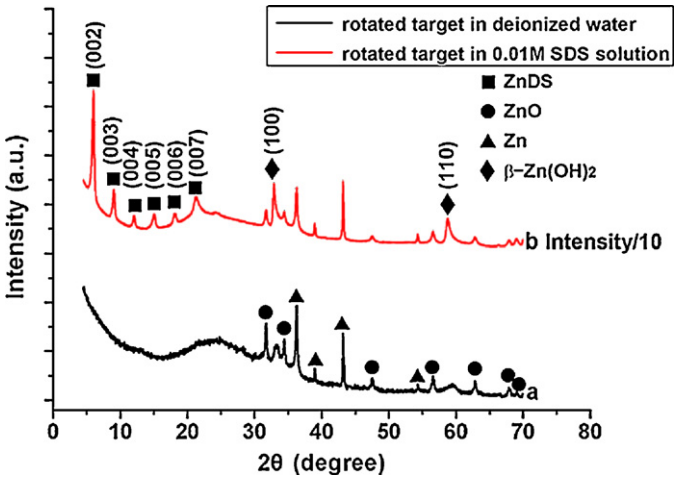

Fig. 1. XRD patterns of products obtained by LAL in liquids of (a) deionized water and (b) a 0.01 M SDS solution using the fundamental nanosecond pulse laser.

were prepared by dispersing the clean powder in ethanol to form a suspension, and then dropping the suspension onto a silicon substrate for SEM or a carbon-coated Cu grid for TEM investigations. A Fourier transform infrared (FT-IR) measurement was conducted on a Thermo Nicolet NEXUS 670 FT-IR Spectrophotometer in the range of 400–4000 cm^{-1}.

2.3. Photoluminescence measurements

PL and SNOM measurements were performed under atmospheric conditions at room temperature. The PL spectra of both colloidal suspensions and dried powder samples were obtained. For PL measurement of colloidal suspensions, repeatedly rinsed, dried powder samples were dispersed in deionized water. For powder sample characterization, ZnHDS nanosheets were dispersed in a no-fluorescence quartz substrate. The 325-nm line of an He–Cd laser was used as the excitation source. For SNOM measurements, an optical fiber probe with an aperture diameter of about 140 nm (supplied by JASCO Corp.) was used as the excitation source to locally excite individual nanostructures. The light emitted from the nanostructures was collected by an objective lens mounted under the substrate, and the integrated light intensity images were measured by introduction of light into a single-photon-counting module. To measure near-field PL spectra, the light emitted from the sample was analyzed with a spectrograph equipped with a liquid-nitrogen-cooled charge-coupled device (CCD) detector. Topographic images of the samples were simultaneously obtained by a shear-force feedback technique. The detection system can efficiently operate over a spectral range of 380–900 nm.

3. Results and discussion

3.1. Phase structure and morphology

Fig. 1a shows the XRD pattern of the products obtained by pulse laser ablation of Zn in pure water (the product assigned as *S-1*). The XRD peaks are clearly ascribed to the metal Zn (JCPDS No. 04-0831) and wurtzite ZnO (JCPDS No. 36-1451) phases. The XRD peaks of Zn are narrow and sharp, indicating relatively larger-sized and better-crystallized metallic Zn structures. Aside from the Zn and ZnO peaks, two weak and broad XRD peaks located at 32.86° and 58.6° in 2θ can be indexed according to a metastable β-$Zn(OH)_2$ structure. The existence of metastable β-$Zn(OH)_2$ with a CdI_2-type structure (a = 3.194 Å, c = 4.714 Å, space group: $D_{3d}{}^3 = \bar{C}3m$) has been confirmed at high pressure [29]. Fig. 1b shows the XRD

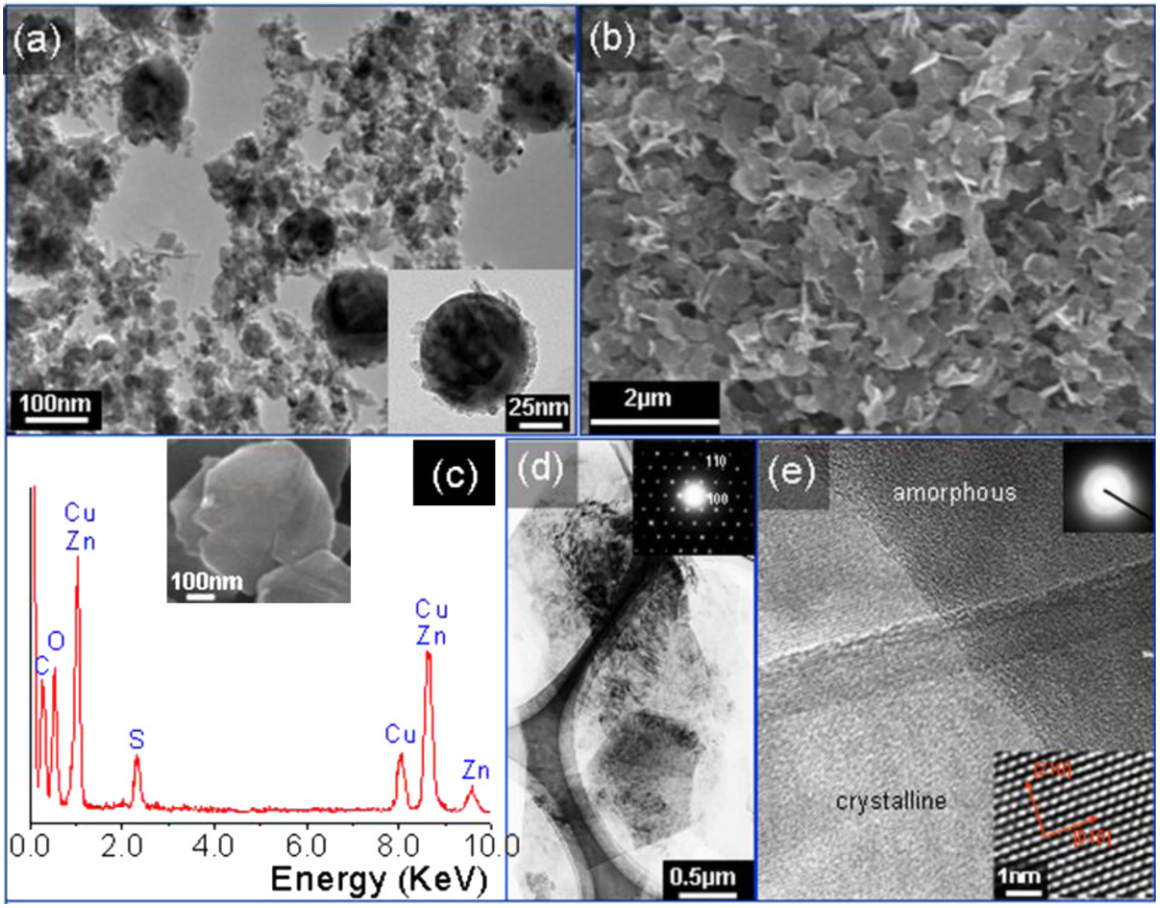

Fig. 2. The morphology and structure of products by LAL of Zn using a 1064-nm laser. (a) TEM image of products by LAL in water, the inset shows a rounded Zn particle coated with ZnO nanoparticles. (b) SEM image of products by LAL in SDS solutions. (c) EDS spectrum of single ZnHDS nanosheet (inset, SEM image) obtained in SDS solutions. (d) TEM image of typical ZnHDS nanosheets, inset is the corresponding single crystalline SAED pattern. (e) HRTEM lattice image of single nanosheet under electron beam irradiation, inset corresponds to the SAED pattern after evolution.

pattern of products obtained from the laser ablation of Zn in 0.01 M SDS solution by continuously rotating the Zn target during ablation (assigned as *S-2*). The intensity value is divided 10 times to obtain a clearer description in the figure. Aside from the Zn, ZnO, and β-$Zn(OH)_2$ diffraction peaks, the remaining peaks in the low angle range can be well indexed to a layered ZnHDS hybrid structure. A series of (0 0 *l*) equally spaced sharp lines present typical evidence of the formation of layered structures with the same basal spacing of 29.32 Å. FT-IR measurements (Fig. S2 in Supplementary Data) for the powder product demonstrate that the ZnHDS nanosheets obtained using the 1064-nm laser present a structure similar to that obtained from third harmonic laser ablation.

Fig. 2 presents typical SEM and TEM images of the products obtained by LAL of Zn in pure water and 0.01 M SDS solution. In the TEM image of *S-1* (Fig. 2a), the product is composed of aggregated particles, large sphere-like particles, and a small amount of sheet-like structures. Selected area electron diffraction (SAED) and energy-dispersive X-ray spectroscopy (EDS) analyses revealed that the aggregated particles are wurtzite ZnO, the large, rounded particles (inset image) are metal Zn surface-coated with fine ZnO nanoparticles, and the sheet-like structures are the β-$Zn(OH)_2$ form, all of which are well in agreement with the XRD analysis.

Fig. 2b presents the products from *S-2*. Most of the products are sheet-like in morphology and rare several small-sized particles are randomly distributed on the surface of some sheets. The ultrathin nanosheets are one to two micrometers in size and nanometers scale in thickness. The EDS spectrum (Fig. 2c) obtained from a single ZnHDS sheet suggests C, O, S, and Zn components. Fig. 2d and e shows the corresponding HRTEM analysis of a single ZnHDS nanosheet. The ZnHDS sheet consists of a β-$Zn(OH)_2$ inorganic layer and organic chains of DS^- molecules in a bi-layer arrangement, the structure of which is schematically depicted in Fig. S3 in the Supplementary Data. The regular shape and SAED pattern along the zone axis of [0 0 1] from a single ZnHDS nanosheet demonstrate the CdI_2-type hexagonal structure of a β-$Zn(OH)_2$ inorganic layer. However, this structure is unstable and easily collapses. Under electron-beam irradiation, the clear lattice image (inset, enlarged image) of the single sheet quickly evolves into an amorphous structure, as verified in the upper HRTEM image and halo rings in the inset SAED pattern (Fig. 2e).

3.2. Photoluminescence properties

Fig. 3 (spectra b and c) shows the PL spectra obtained from the colloidal suspensions of *S-1* and *S-2*. In all spectra, the peaks located at 367 nm are attributed to the Raman scattering of water, as evidenced in the measurement for pure water (spectrum a). In *S-1*, aside from weak UV-band emission at 380 nm and a very broad green band emission located at 550 nm, weak emission peaks are observed at around 445 and 470 nm. In *S-2*, remarkably enhanced PL emissions in the blue region are observed with three typical sub-band peaks located at 413, 445, and 471 nm. In *S-2*, evident green emissions with peak centers at 550 nm are also present, the intensities of which are increased compared with that in *S-1*; however, the UV-band emission here is obviously quenched. The inset in Fig. 3 presents a photograph of colloidal samples obtained by LAL of Zn in

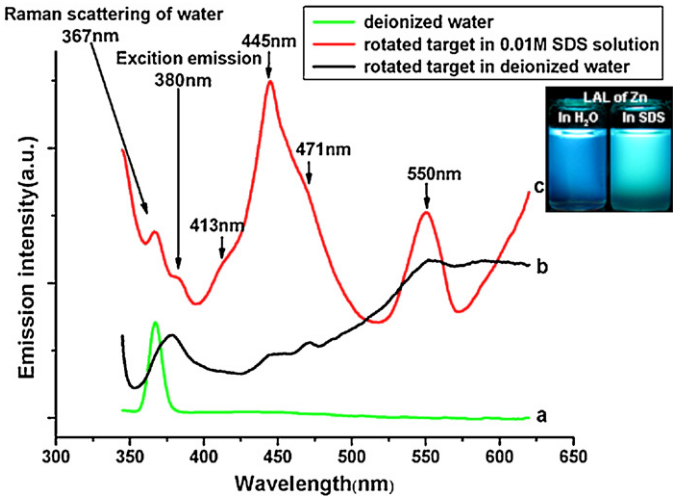

Fig. 3. PL spectra of (a) pure water, (b) colloidal suspensions induced by LAL in deionized water, and (c) colloidal suspensions induced by LAL in 0.01 M SDS solution. Inset shows a photograph of colloidal *S-1* and *S-2* under UV-light illumination. Excitation wavelength: 325 nm.

pure water and 0.01 M SDS solution under UV light excitation; the left bottle presents evident violent-blue emissions from colloidal *S-1*, while the right bottle presents blue-green emissions from *S-2*. Based on the XRD and TEM investigations, the UV-band emission in *S-1* could clearly be attributed to the band-gap or the excitonic emission of ZnO nanoparticles, while the green band emission may have resulted from ZnO nanoparticles with rich, individual ionized oxygen vacancies or zinc interstitials defects. The multiple-band blue emissions in *S-1* are very possibly caused by the metastable β-$Zn(OH)_2$ phase. This is further confirmed in *S-2*, after assembly with DS^- ions to form ZnHDS layered nanosheets, where the intensity of blue emissions is dramatically enhanced.

The PL spectra of the colloidal solutions suggest that the ZnHDS nanosheets also contribute to the enhanced green band emission in *S-2*. In the current study, we intentionally removed the large Zn sphere phase from the colloidal solutions by repeated centrifugation. Fig. S4 in the Supplementary Data (Fig. S4a) presents the XRD spectrum of the product after removal of Zn spheres. The corresponding PL spectrum from ZnHDS containing colloidal solutions was recorded, as shown in Fig. S4b. Clearly, ZnHDS nanosheets present strong blue and green bands emissions; the very weak peak at about 380 nm could be the band-gap or excitonic emission from trace amounts of ZnO nanoparticles. The SDS solution does not show PL emissions, as shown in Fig. S5 of the Supplementary Data. The colloidal solutions measured for PL do not contain free SDS molecules after repeated centrifugation and rinsing, as demonstrated in the XRD analysis; the XRD peaks of SDS molecules could not be detected.

Aside from investigating the PL properties of an ensemble from colloidal solutions, we also investigated PL emissions from individual ZnHDS nanosheets using the nanoscale SNOM technique. The ZnHDS nanosheets obtained from a colloidal suspension were dispersed through a commercially purchased no-luminescence quartz substrate, and then dried at room temperature. Since these ultrathin nanosheets are not completely flat on the substrate, some parts of nanosheet are curved, and some parts overlap each other. Fig. 4a and b shows the typical shear force image of individual ZnHDS nanosheets and the corresponding integrated light intensity image, respectively. The contrast difference in Fig. 4a is caused by the height profile of the ZnHDS sheet and the varied distance between probe tip and different spots on nanosheets, while the contrast difference in the integrated light intensity image of Fig. 4b reflects the variation of emission intensity. Fig. 4c gives the near-field PL spectra obtained from the three positions, as labeled in Fig. 4b. Although the total intensity is not as large as that from the colloidal sample, sub-emission bands with centers at 418, 443, 479, and 543 nm are clearly well in agreement with those in the spectra of colloidal *S-2* due to the integration of a single nanosheet emission. Both the ensemble and individual PL measurements demonstrate that ZnHDS nanosheets display enhanced blue and green emissions under UV-light excitation.

The measurements above suggest that β-$Zn(OH)_2$, as an inorganic layer, plays critical roles in the unusual blue emission from the ZnHDS structure. β-$Zn(OH)_2$ exhibits a typical CdI_2-type structure, in which the OH^- anions form a hexagonal, close-packed arrangement, whereas the Zn cations fill all of the octahedral sites in alternate layers. The β-$Zn(OH)_2$ structure is mostly ionically bonded, but retains a partially covalent character. This structure is analogous to that of wurtzite ZnO, and belongs to the polar crystal class. The main difference between the two structures is that the Zn cations are covalently bonded with OH radicals in β-$Zn(OH)_2$. The unusual blue emission in hybrid ZnO/organic composites can only be observed in highly basic solutions, thus, the bonding of OH radicals may participate in the blue emissions of hybrid ZnO/organic composites. For example, Fu et al. demonstrated that the hydroxyl groups on the surface of ZnO nanoparticles react with organic molecules and only thus assembled composite show strong blue emission [30]. Our finding of blue luminescence from non-stoichimetric β-$Zn(OH)_{2-x}$ may give indication about the critical role of hydroxyl groups on the surface of ZnO nanoparticles. Similarly, the Zn–OH–DS bonded surface states could be the origin for strong blue emission in ZnHDS composite. Determination of a calculation theory for clarifying the band gap structure of β-$Zn(OH)_2$ would be desirable in future study.

3.3. Formation process for hybrid ZnHDS nanosheet by LAL in SDS solution

XRD and TEM investigations demonstrate that varied structures may be obtained by LAL of Zn, suggesting that different growth processes may be responsible for the production of metallic Zn spheres, fine ZnO nanoparticles, and layered ZnHDS hybrid nanosheets. The liquid-confinement in LAL makes direct diagnostics of the ejected species very challenging. The strong interaction of the species with the liquid eliminates evidence of the primary ejection mechanism; only secondary processes are generally observed [31]. Investigations of surface morphology may be the best tool for identifying materials, and distinguishing between surface vaporization and the direct ejection of materials from molten surfaces [31,32].

Fig. 5a shows SEM images of ablation regions on the surface of the Zn target using a 1064-nm laser wavelength. Large, deep craters with diameters of 10–20 μm (see inserted enlarged image) are randomly distributed within the irradiated area. The size of the craters is much smaller than the laser focus spot (1.0 mm). The inset (enlarged SEM image) indicates that the craters are concentrated in regions where melting has occurred, suggesting that the surface melts locally and that large vapor bubbles are formed and released in these portions. In our previous report, however, almost pure ZnHDS layered nanocomposites could be obtained by laser ablation of Zn in SDS solutions using the third harmonic line of an Nd:YAG laser [16]. Fig. 5b shows SEM images of the morphology of a rotated Zn target surface after LAL using a 355-nm laser wavelength. Randomly dispersed swirl textures are formed with diameters of around 10 μm, as shown in the inset (enlarged image). Moreover, many nanometer-scale pores appear. In the laser ablation of a target using a nanosecond pulse laser, two typical processes for the removal of materials from the target surface have been recognized [33], i.e., thermal vaporization of atomic or ionic

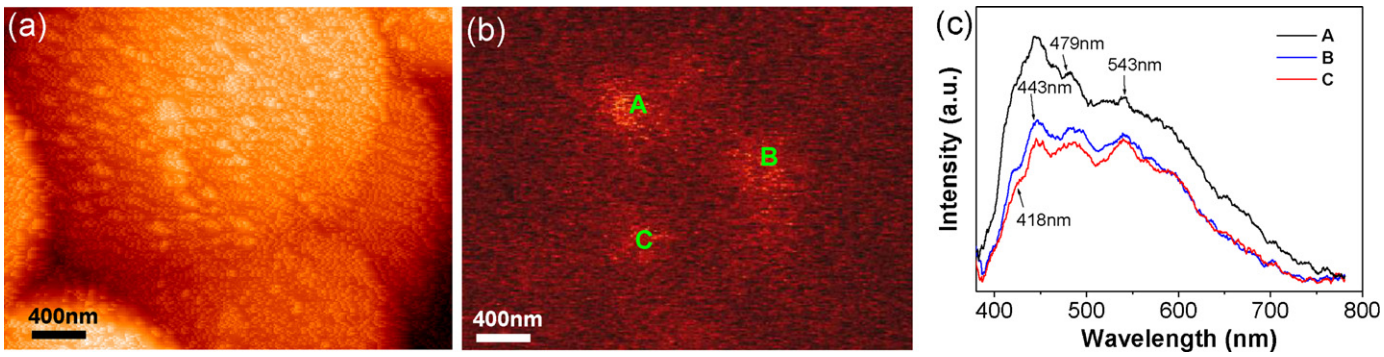

Fig. 4. SNOM characterization of a single layered ZnHDS nanosheet. (a) Shear force image of individual ZnHDS nanosheets, (b) the corresponding integrated light intensity image of the nanosheet, and (c) the near-field spectra measured at three positions on the nanosheet, as labeled in (b).

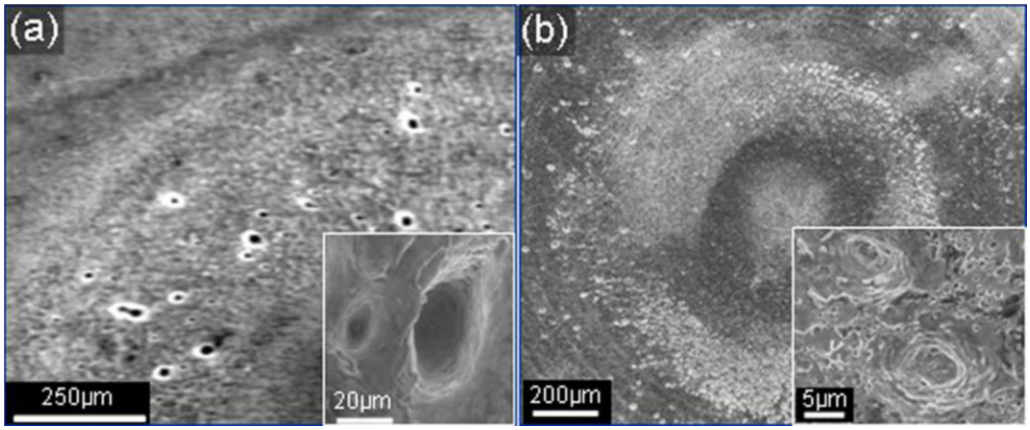

Fig. 5. SEM images of the Zn target surface after LAL in SDS solutions: (a) ablation using 1064-nm laser wavelength, inset image shows large craters and (b) ablation using 355-nm laser wavelength, inset image shows swirl texture-like morphology.

species and thermally induced explosive ejection of nanometer- or micrometer-sized molten droplets from the heated target.

Evidently, for LAL using the fundamental nanosecond pulse laser, both processes may occur. The molten Zn droplets could quench and solidify as Zn spheres, while nanosize Zn droplets may also oxidize into ZnO nanoparticles. Thermal vaporization generates Zn species that could react with H_2O to form zinc hydroxide species. These zinc hydroxide species can further transform into ZnO nanoparticles. However, in the presence of DS^- ions, these zinc hydroxide species could cause charge–assemblies to form ZnHDS layered nanosheets. The formulas below represent the main reactions that may occur in water or SDS solutions by LAL.

$$Zn + (2-x)H_2O \rightarrow Zn(OH)_{2-x}{}^{x+} + (2-x)H^+ \quad (1)$$

$$Zn(OH)_{2-x}{}^{x+} + x/4O_2 \rightarrow ZnO + (1-1/2x)H_2O \quad (2)$$

$$Zn(OH)_{2-x}{}^{x+} + xDS^- \rightarrow Zn(OH)_{2-x}DS_x \quad (3)$$

For Zn ablation using third harmonic nanosecond lasers, however, no large craters and Zn metal droplets appeared, indicating that the ejection of Zn species, as result of thermal vaporization, could be the main process.

4. Conclusions

We investigated the formation of layered ZnHDS hybrid nanosheets using a fundamental nanosecond Nd:YAG pulse laser in the liquid-phase laser ablation of Zn. In SDS solutions, hybrid ZnHDS nanosheets could be fabricated in significant amounts. Investigations after ablation revealed microscale craters on the target surface after using a 1064-nm laser, whereas swirl textures and nanometer-scale pores appeared using a 355-nm laser. Thermally induced vaporization of Zn species is favorable for the formation of ZnHDS nanosheets in SDS solutions and ZnO nanoparticles in pure water, while the explosive boiling and ejection of melting Zn droplets is responsible for the formation of sphere-like Zn particles. PL measurements of colloidal suspensions in an ensemble and SNOM light-emission detection of single ZnHDS nanosheets revealed metastable β-$Zn(OH)_2$ structures with multiple-band blue and green emissions, the intensities of which were remarkably enhanced after assembling with DS^- molecules into hybrid ZnHDS nanosheets. The unique LAL technique, which employs metallic target and organic solutions, are expected to be able to synthesize other hybrid organic–inorganic structures. Uniform layered ZnHDS nanosheets with strong and stable visible-light emissions show promise in future applications as new luminescent materials.

Acknowledgments

This work was financially supported by the National Natural Science Foundation of China (Grant Nos. 10974204 and 50931002), the National Basic Research Program of China (Grant 2007CB936603) and the Hundred Talent Program of the Chinese Academy of Sciences.

Appendix A. Supplementary data

Supplementary data associated with this article can be found, in the online version, at doi:10.1016/j.jphotochem.2011.09.013.

References

[1] G.W. Yang, Laser ablation in liquids: applications in the synthesis of nanocrystals, Prog. Mater. Sci. 52 (2007) 648–698.
[2] S. Barcikowski, F. Devesa, K. Moldenhauer, Ablation of noble metals in liquids: a method to obtain nanoparticles in a thin polymeric film, J. Nanopart. Res. 11 (2009) 1883–1893.
[3] M. Shoji, K. Miyajima, F. Mafune, Ionization of gold nanoparticles in solution by pulse laser excitation as studied by mass spectrometric detection of gold cluster ions, J. Phys. Chem. C 112 (2008) 1929–1932.
[4] S. Barcikowski, A. Menendez-Manjon, B. Chichkov, M. Brikas, G. Raciukaitis, Generation of nanoparticle colloids by picosecond and femtosecond laser ablations in liquid flow, Appl. Phys. Lett. 91 (2007) 083113.
[5] T. Tsuji, K. Iryoa, N. Watanabe, Preparation of silver nanoparticles by laser ablation in solution influence of laser wavelength on particle size, Appl. Surf. Sci. 202 (2002) 80–85.
[6] H.M. Zhang, C.H. Liang, Z.F. Tian, G.Z. Wang, W.P. Cai, Single phase Mn_3O_4 nanoparticles obtained by pulsed laser ablation in liquid and their application in rapid removal of trace pentachlorophenol, J. Phys. Chem. C 114 (2010) 12524–12528.
[7] X.Q. Li, W.X. Zhang, Sequestration of metal cations with zerovalent iron nanoparticles—a study with high resolution X-ray photoelectron spectroscopy (HR-XPS), J. Phys. Chem. C 111 (2007) 6939–6946.
[8] J.N. Anker, W.P. Hall, O. Lyandres, N.C. Shah, J. Zhao, R.P. Van Duyne, Biosensing with plasmonic nanosensors, Nat. Mater. 7 (2008) 442–453.
[9] S. Petersen, S. Barcikowski, In situ bioconjugation: single step approach to tailored nanoparticle-bioconjugates by ultrashort pulsed laser ablation, Adv. Funct. Mater. 19 (2009) 1167–1172.
[10] G. Compagnini, A.A. Scalisi, O. Puglisi, Ablation of noble metals in liquids: a method to obtain nanoparticles in a thin polymeric film, Phys. Chem. Chem. Phys. 4 (2002) 2787–2791.
[11] C.H. Liang, Y. Shimizu, T. Sasaki, N. Koshizaki, Synthesis of ultrafine SnO_{2-x} nanocrystals by pulsed laser-induced reactive quenching in liquid medium, J. Phys. Chem. B 107 (2003) 9220–9225.
[12] C.H. Liang, Y. Shimizu, T. Sasaki, N. Koshizaki, Pulsed-laser ablation of Mg in liquids: surfactant-directing nanoparticle assembly for magnesium hydroxide nanostructures, Chem. Phys. Lett. 389 (2004) 58–63.
[13] S. Link, C. Burda, B. Nikoobakht, M.A. El-Sayed, Laser-induced shape changes of colloidal gold nanorods using femtosecond and nanosecond laser pulses, J. Phys. Chem. B 104 (2000) 6152–6163.
[14] T. Tsuji, T. Hamagami, T. Kawamura, J. Yamaki, M. Tsuji, Laser ablation of cobalt and cobalt oxides in liquids: influence of solvent on composition of prepared nanoparticles, Appl. Surf. Sci. 243 (2005) 214–219.
[15] C.H. Liang, Y. Shimizu, T. Sasaki, N. Koshizaki, Synthesis, characterization, and phase stability of ultrafine TiO_2 nanoparticles by pulsed laser ablation in liquid media, J. Mater. Res. 19 (2004) 1551–1557.
[16] C.H. Liang, Y. Shimizu, M. Masuda, T. Sasaki, N. Koshizaki, Preparation of layered zinc hydroxide/surfactant nanocomposite by pulsed-laser ablation in a liquid medium, Chem. Mater. 16 (2004) 963–965.
[17] C. He, T. Sasaki, Y. Shimizu, N. Koshizaki, Synthesis of ZnO nanoparticles using nanosecond pulsed laser ablation in aqueous media and their self-assembly towards spindle-like ZnO aggregates, Appl. Surf. Sci. 254 (2008) 2196–2202.
[18] L. Yang, P.W. May, L. Yin, T.B. Scott, Growth of self-assembled ZnO nanoleaf from aqueous solution by pulsed laser ablation, Nanotechnology 18 (2007) 215602.
[19] Y. Ishikawa, C.H. Liang, Y. Shimizu, T. Sasaki, N. Koshizaki, Preparation of zinc oxide nanorods using pulsed laser ablation in water media at high temperature, J. Colloid Interface Sci. 300 (2006) 612–615.
[20] P. Wagener, A. Schwenke, B.N. Chichkov, S. Barcikowski, Pulsed laser ablation of zinc in tetrahydrofuran: bypassing the cavitation bubble, J. Phys. Chem. C 114 (2010) 7618–7625.
[21] Z.J. Yan, R.Q. Bao, D.B. Chrisey, Self-assembly of zinc hydroxide/dodecyl sulfate nanolayers into complex three-dimensional nanostructures by laser ablation in liquid, Chem. Phys. Lett. 497 (2010) 205–207.
[22] M. Bdullah, T. Morimoto, K. Okuyama, Generating blue and red luminescence from ZnO/Poly(ethylene glycol) nanocomposites prepared using an in-situ method, Adv. Funct. Mater. 13 (2003) 800–804.
[23] T.G. Jiu, H.B. Liu, L.M. Fu, X.R. He, N. Wang, Y.L. Li, X.C. Ai, D.B. Zhu, Novel blue-light-emitting hybrid materials based on oligothiophene acids and ZnO, Chem. Phys. Lett. 398 (2004) 113–137.
[24] Q.T. Wang, X.B. Wang, W.J. Lou, J.C. Hao, Stable blue- and green-emitting zinc oxide from ionic liquid crystal precursors, ChemPhysChem 10 (2009) 3201–3203.
[25] H.M. Xiong, D. Liu, Y. Xia, J. Chen, Polyether-grafted ZnO nanoparticles with tunable and stable photoluminescence at room temperature, Chem. Mater. 17 (2005) 3062–3064.
[26] O. Altuntasoglu, Y. Matsuda, S. Ida, Y. Matsumoto, Syntheses of zinc oxide and zinc hydroxide single nanosheets, Chem. Mater. 22 (2010) 3158–3164.
[27] T. Tsuruoka, C.H. Liang, K. Terabe, T. Hasegawa, Origin of green emission from ZnS nanobelts as revealed by scanning near-field optical microscopy, Appl. Phys. Lett. 92 (2008) 091908.
[28] T. Tsuruoka, C.H. Liang, K. Terabe, T. Hasegawa, Optical waveguide properties of single indium oxide nanofibers, J. Opt. A: Pure Appl. Opt. 10 (2008) 055201.
[29] M.I. Baneyeva, S.V. Popova, A study of zinc hydroxide at high pressures and temperatures, Geochem. Int. USSR 6 (1969) 807–809.
[30] Y.S. Fu, X.W. Du, S.A. Kulinich, J.S. Qiu, W.J. Qin, R. Li, J. Sun, J. Liu, Stable aqueous dispersion of ZnO quantum dots with strong blue emission via simple solution route, J. Am. Chem. Soc. 129 (2007) 16029–16033.
[31] R. Kelly, in: D.B. Chrisey, G.K. Hubler (Eds.), Pulsed Laser Deposition of Thin Films, Wiley, New York, 1994.
[32] W.T. Nichols, T. Sasaki, N. Koshizaki, Laser ablation of a platinum target in water. I. Ablation mechanisms, J. Appl. Phys. 100 (2006) 114911.
[33] T.D. Bennett, C.P. Grigoropoulos, D.J. Krajnovich, Near-threshold laser sputtering of gold, J. Appl. Phys. 77 (1995) 849–864.